International Journal of Advances in Engineering and Management (IJAEM)
Volume 6, Issue 10 Oct. 2024, pp: 214-229www.ijaem.net ISSN: 2395-5252

Design and Performance Analysis of Reconfigurable Millimetre-Wave Metamaterial Antenna for 5G Wireless Applications

Uduak S. Ubia[1], Kufre M. Udofia[2] and Akaninyene B. Obot[3]
[1,2,3]*Department of Electrical and Electronics Engineering, University of Uyo, Uyo, Nigeria.*

Date of Submission: 10-10-2024 Date of Acceptance: 20-10-2024

ABSTRACT: The development of fifth generation (5G) and beyond wireless technology necessitated advancements in antenna design to meet the high-frequency requirements and bandwidth demands of millimetre-wave (mm-Wave) communications. This research focused on the design and performance analysis of a reconfigurable mm-Wave antenna tailored for 5G applications, specifically targeting frequencies at 26, 28, and 30 GHz. Three single-band microstrip antennas were designed, simulated, and analysed based on fundamental antenna parameters, including return loss, VSWR, radiation pattern, directivity, and gain. The proposed antenna features a reconfigurable mechanism utilizing diodes to switch between different operational states, thereby modifying the antenna's bandwidth and performance characteristics. Inductance of 0.5 nH and resistance of 1Ω as well as 1 MΩ resistance were used for both ON and OFF states, respectively. When the diode was activated (ON state), the antenna achieved a bandwidth of 2.56 GHz. Conversely, in the OFF state, the antenna provided a slightly reduced bandwidth of 2.23 GHz. This reconfigurability allowed the antenna to dynamically adapt to varying communication scenarios and frequency requirements, enhancing its versatility and effectiveness in 5G networks. The design incorporated metamaterial and precise design to ensure optimal performance across the specified frequency bands. Performance metrics, including return loss, gain, and radiation patterns, have been meticulously analysed to validate the antenna's suitability for high-speed, high-frequency 5G applications. Overall, the reconfigurable mm-Wave antenna demonstrated significant potential in improving the adaptability and efficiency of 5G wireless communication systems, offering robust performance across multiple key frequency bands with considerable bandwidths in both diode states.

KEYWORDS: Metamaterial, mm-Wave, reconfigurable, 5G, diode

I. INTRODUCTION

The progression from the long-term evolution (LTE) of cellular communications to the generally perceived future generation (mainly the fifth generation of mobile communication), as acceded to by [1], is mainly spurred on by the growing need for improved data rate (gigabytes per second) and lower latency in an expanded range of applications. However, with the quest for reduced latency and improved speed comes the challenge of diminishing frequency spectrum, which has forced the transition of wireless communication to extremely high frequencies (EHF) [2]. Ref [3] reported that despite the huge bandwidth available for data communication in the EHF frequency range, they are known to be severely plagued by short wavelength (in millimetres), which had primarily delayed their speed of adoption contrary to the previous generations. Alternative frequencies (especially C-band) have been used to deploy the 5G technology by network providers as a countermeasure to the short wavelength of EHF [4]– [6]. In their submission, [7] stated that these alternative frequencies adopted for 5G faced data speed and latency constraints compared to those in mm-wave transmission.

According to [8], reconfigurable mm-wave antennas are expected to bridge the wide adoption of wireless networks' 5G and beyond technology. This assertion holds true mainly because these categories of antennas can dynamically be modified to suit desired application requirements using discrete circuit components like

International Journal of Advances in Engineering and Management (IJAEM)
Volume 6, Issue 10 Oct. 2024, pp: 214-229www.ijaem.net ISSN: 2395-5252

diodes, capacitors, varactors, variable resistors, inductors, and, in some cases, transformers [9].

This study proposes the design and performance analysis of reconfigurable metamaterial antenna for 5G mm-wave communications. The antenna will be designed in stages, starting with a microstrip antenna as a building template before optimising the reflector geometry with suitable components for reconfiguration. Also, the bandwidth and polarisation properties of the antenna will be investigated using a defected ground structure and metamaterial.

II. REVIEW OF RELATED LITERATURES

A review of some recently published research papers related to this study is presented as follows.

For 5G connectivity, [10] proposed a cutting-edge design of a 30 GHz microstrip quarter-fed antenna using Rogers RT5880 substrate. The antenna used a C-shaped slit that measured 0.4 mm. The authors reported an antenna gain of 8.45 dB, directivity of 5^0, VSWR of 2.3, bandwidth of 3.5 GHz, and a reflection coefficient of -8 dB at a resonant frequency of 30 GHz based on measurements. However, the reported VSWR value of 2.3 exceeds the permitted standard performance metrics (the acceptable value is 1<VSWR<2).

El Hadri [8] integrated U- and T-shaped antenna architecture with two-state geometry in their design of a reconfigurable antenna for 5G mm-Wave and Wireless Fidelity (Wi-Fi) applications. This was done in order to improve bandwidth and achieve two-mode operation. The U-shaped structure was directly connected to the T-shaped geometry containing the feedline in the first state. Their proposed antenna with dimensions of 30 mm×26.5 mm×1.6 mm was printed on an FR-4 substrate with a dielectric constant of 4.4. A bandwidth of 2.57 GHz was reported at a resonance frequency of 28.02 GHz. The authors' choice of reconfiguration was not electronically regulated.

Ref [11] developed a new, small frequency reconfigurable antenna for millimetre wave communications. The authors achieved a large operational bandwidth by combining complementary split ring resonators and a defective ground construction. They reported a return loss at frequency range of 20.75–37.8 GHz (S_11<-10 dB), with a maximum bandwidth of 17.05 GHz. Three PIN diodes, D_1, D_2 and D_3, were inserted between slots in the radiating structure to switch frequencies. It was possible to achieve both wide and narrow operating bands within 20 and 38 GHz for different combinations of PIN diodes in the ON-OFF states. Their proposed antenna produced a radiation efficiency of 96% over the working bands at a peak gain of 6 dB. All antenna parameters reported by the authors lacked visual depictions.

The concept of a hexagonal patch antenna inscribed in a unit cell split-ring resonator (SRR) and reconfigured using two PIN diodes for mm-wave 5G application was presented by [12]. In order to create a metamaterial structure that lessen mutual coupling between antenna elements, the authors reported that SRR was utilised. The authors employed the diodes to achieve a four-mode operation, and they were labelled 10, 01, 00, and 11 to denote the order of connection of the diodes to the 3×3 array antenna. The substrate used had a 30 mm × 23 mm size. From their report, at a resonance frequency of 27.8 GHz and antenna mode 11, a maximum antenna gain of 4 dB was achieved. The substrate used for the antenna design was not mentioned. Additionally, none of the antenna modes taken into consideration underwent an antenna reconfiguration at frequencies greater than 25.8 GHz.

The article by [13] discussed reconfigurable antennas for millimetre waves. A 24 GHz active printed antenna array was created and fed into an inhomogeneous lens in order to obtain reconfigurable patterns, specifically sectorial and directional situations (Half Maxwell Fish Eye). In the first section, the authors described a multilayer active array with four patches. The array helped to manage the radiation pattern by giving each element a commutator and changing the number of feed patches. Additionally, the array was put into an inhomogeneous lens to produce the radiation pattern in the second part. The research was focused on radiation pattern reconfiguration while the suggested antenna in this study is focused on frequency reconfiguration for multiband.

III. METHODOLOGY

3.1 Design Considerations for Rectangular Microstrip Antenna

The design of three single-band microstrip antennas adopts the standard transmission line equations as presented by [14], [15]. The physical dimensions of the microstrip, such as the width, length, and dimensions of the microstrip line, are calculated using the following equations:

The width of the patch W_p is determined from Equation 1:

$$W_p = \frac{c}{2f_r}\sqrt{\frac{2}{\varepsilon_r+1}} \quad (1)$$

where c, f_r and ε_r are the speed of light, design

International Journal of Advances in Engineering and Management (IJAEM)
Volume 6, Issue 10 Oct. 2024, pp: 214-229www.ijaem.net ISSN: 2395-5252

frequency and relative permittivity.

The patch length is calculated using Equation 4, however, the length's extension, ΔL and the effective permittivity, ε_{reff} are first calculated from Equations 2 and 3 before the length of the microstrip patch. The substrate thickness, h of 1.6 mm, is maintained throughout the design. The effective dielectric constant and length extension are calculated thus:

$$\varepsilon_{reff} = \frac{\varepsilon_r+1}{2} + \frac{\varepsilon_r-1}{2}\left[1+12\frac{h}{W_p}\right]^{-\frac{1}{2}} \quad (2)$$

$$\Delta L = 0.412h\,\frac{(\varepsilon_{reff}+0.3)\left[\frac{W_p}{h}+0.264\right]}{(\varepsilon_{reff}-0.258)\left[\frac{W_p}{h}+0.8\right]} \quad (3)$$

The patch length is calculated from Equation 4 thus:

$$L = \frac{c}{2f_r\sqrt{\varepsilon_{reff}}} - 2\Delta L \quad (4)$$

As earlier stated, inset feeding technique was used to offset the feeding location to the point where an impedance match between the patch and feedline can be achieved. The inset feed parameters are determined using the following equations.

To calculate the notch width, g equation from [12] is employed as given in Equation 5.

$$g = \frac{c\, f_r \times 10^{-9} \times 4.65 \times 10^{-9}}{\sqrt{2\varepsilon_{reff}}} \quad (5)$$

The resonant input resistance R_{in} is calculated from Equation 6;

$$R_{in}(y=y_o) = \frac{1}{2(G_1+G_{12})}\cos^2\left(\frac{\pi y_o}{L_p}\right) \quad (6)$$

The equation for the characteristic impedance Z_o is given in Equation 7;

$$Z_0 = \begin{cases} \frac{60}{\sqrt{\varepsilon_{reff}}}\ln\left[\frac{8h}{W_f}+\frac{W_f}{4h}\right] & \text{for } \frac{W_f}{h} \le 1 \\ \frac{120\pi}{\sqrt{\varepsilon_{reff}}}\left[\frac{W_f}{h}+1.393+0.667\ln\left(\frac{W_f}{h}+1.444\right)\right] & \text{for } \frac{W_f}{h} \ge 1 \end{cases} \quad (7)$$

In this design, the ratio, $\frac{W_f}{h} = \frac{2.98}{1.6} = 1.863 > 1$, so the second expression in Equation 7 applies.

Edge impedance, $R_{in(edge)}$ is computed from Equation 8.

$$R_{in(edge)} = \frac{1}{2(G_1 \mp G_{12})} \quad (8)$$

As reported by [15], the plus (+) sign is used for modes with odd (antisymmetric) resonance voltage distribution beneath the patch and between the slots, while the minus (-) sign is used for modes with even symmetric resonant voltage distribution. Other parameters such as wave number k, input current I1, input conductance G1, and mutual conductance G12 must first be known to evaluate the input resistance. The equations for computing the various parameters highlighted are given in Equations 9 to 13.

$$k = \frac{2\pi}{\lambda_{air}} \quad (9)$$

$$I_1 = -2 + \cos(X) + XS_i(X) + \frac{\sin(X)}{X} \quad (10)$$

$$X = kW_p \quad (11)$$

$$G_1 = \frac{I_1}{120\pi^2} \quad (12)$$

$$G_{12} = \frac{1}{120\pi^2}\int_0^{\pi}\left[\frac{\sin(\frac{kW_p}{2}\cos\theta)}{\cos\theta}\right]^2 J_o(kL_p\sin\theta)\sin^3\theta\, d\theta \quad (13)$$

where J_o is the Bessel function of the first kind of order zero. G_{12} is resolved using MATLAB script to calculate rectangular microstrip antenna parameters.

Inset feed technique is used with a chosen characteristic impedance of 50 Ω. [14]

The length of the ground plane (L_g) is:

$$L_g = 6h + L_p \quad (17)$$

The width of the ground plane is:

$$W_g = 6h + W_p \quad (18)$$

The geometry of the designed single-band RMSAs is depicted in the schematic diagram presented in Fig. 1, while the computed values are presented in Table 1.

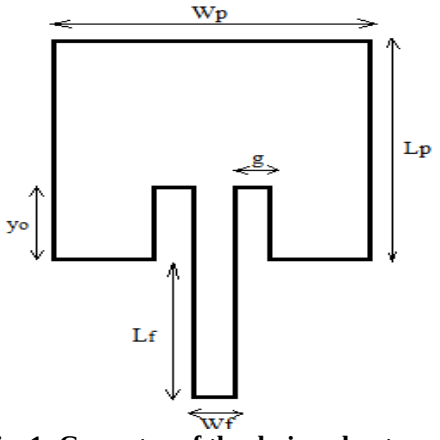

Fig. 1: Geometry of the designed antenna

The selected substrate for the proposed antenna design is RT/Duriod 5880 with substrate height, h of 0.34 mm and patch thickness, t of 0.035 mm.The computed dimensions at the considered frequencies are presented in Table 1. The modelled antennas in computer simulation studio (CST) are presented in Fig. 2

International Journal of Advances in Engineering and Management (IJAEM)
Volume 6, Issue 10 Oct. 2024, pp: 214-229www.ijaem.net ISSN: 2395-5252

Table 1: Computed dimension of single band antennas at 26, 28 and 30 GHz

DESIGN PARAMETER	26 GHz	28 GHz	30 GHz
L_p	3.69 mm	3.41 mm	3.16 mm
W_p	4.56 mm	4.24 mm	3.95 mm
L_g	5.73 mm	5.45 mm	5.20 mm
W_g	6.60 mm	6.28 mm	5.99 mm
W_f	1.06 mm	1.06 mm	1.05 mm
L_f	1.02 mm	0.78 mm	0.51 mm
R_{in}	238.19 Ω	236.30 Ω	230.62 Ω
g	0.14 mm	0.14 mm	0.12 mm
y_o	1.19 mm	1.14 mm	1.10 mm

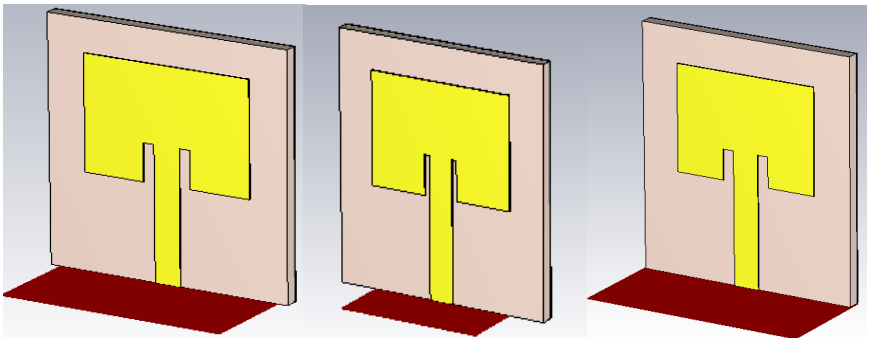

(a) (b) (c)

Fig. 2: Single band antennas in CST Studio (a) 26 GHz (b) 28 GHz (c) 30 GHz

3.2Design Considerations for Antenna Reconfiguration and Parasitic Patch

An antenna that can alter its electrical characteristics following the frequency of operation is called a reconfigurable antenna. The PIN diode reconfiguration is preferred in this design due to its advantages over other switching mechanisms, such as higher supply voltage, shorter switching times, and lower cost [16]. Accordingly, in the mm-Wave frequency range, PIN diodes are noted to be the most utilised electrical switching method in that they function as variable resistors in RF circuits [17]. The analogous circuit for a PIN diode in the ON and OFF states is shown in Fig. 3.

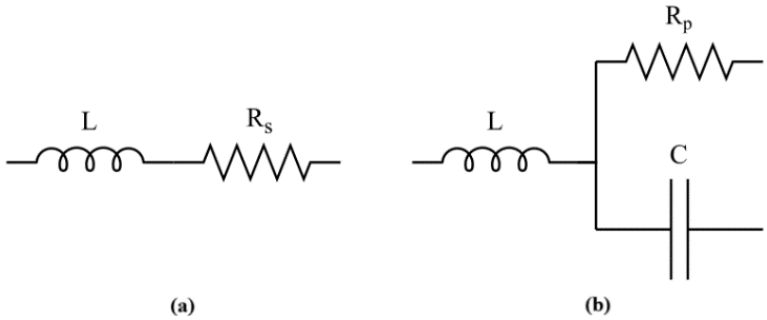

(a) (b)

Fig. 3: Analogous circuit of a PIN diode (a) ON state (b) OFF state [17]

For both ON and OFF modes, the inductance L has the same value (0.5 nH for the design in view). However, in the ON state, a tiny value of the series resistance Rs (1Ω) permits current flow, whereas in the OFF state, a large value of the parallel resistance Rp (1 $M\Omega$) results in an open circuit behaviour. This can be represented in full-wave modelling as a lumped RLC border as illustrated in Fig. 3 (a) and (b).

3.3Design Considerations for Secondary Patch

According to[18], though the secondary patch maintains the same width (W_p) as the primary patch, and $\frac{L_p}{2}$ as length depending on the

International Journal of Advances in Engineering and Management (IJAEM)
Volume 6, Issue 10 Oct. 2024, pp: 214-229www.ijaem.net ISSN: 2395-5252

application, the spacing between these patches are kept to a minimum, noting that the best bandwidth is achieved by strategically cutting gaps of hexagonal and circular shapes inside the patches. Fig.4 gives the proposed antenna design in CST Studio.

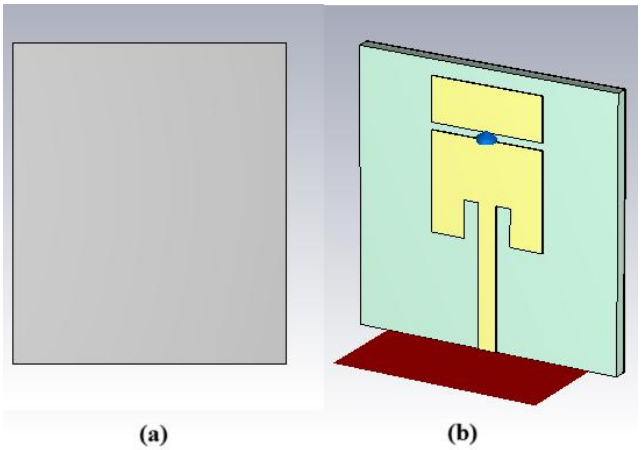

Fig.4: Proposed reconfigurable antenna in CST MWS (a) back view (b) front view

3.4Design Considerations for Unit Cell Metamaterial (MTM)

Varying the shape and dimensions of a unit cell yields varied values of permeability (μ), resonant frequencies (f_r) and permittivity (ε). The sizes of each unit cell type makes modification feasible to meet the criterion at the frequency of resonance, denoted as f_r[19]. Ref [20] stated that the size of the unit cell is about one-tenth of the functional wavelength in air, denoted as λ_{air}. This means that when extracting effective parameters from reflection and transmission data, it is crucial for the unit-cell dimension to be smaller than the operating wavelength. Therefore, by considering one-tenth of the wavelength of the smallest antenna (30 GHz antenna) as the external length, denoted as L_m, the external ring length of the metamaterial (MTM) is calculated to be 1 mm.

$$L_m = \frac{10}{10}$$
$$= 1\ mm$$

The preferred MTM shape for this study is the square split ring resonator (SSRR) due to its simplicity in design and analysis.The dimensions of the unit cell metamaterial are given in Table 2 while the designed SSRR is given in Fig. 5.

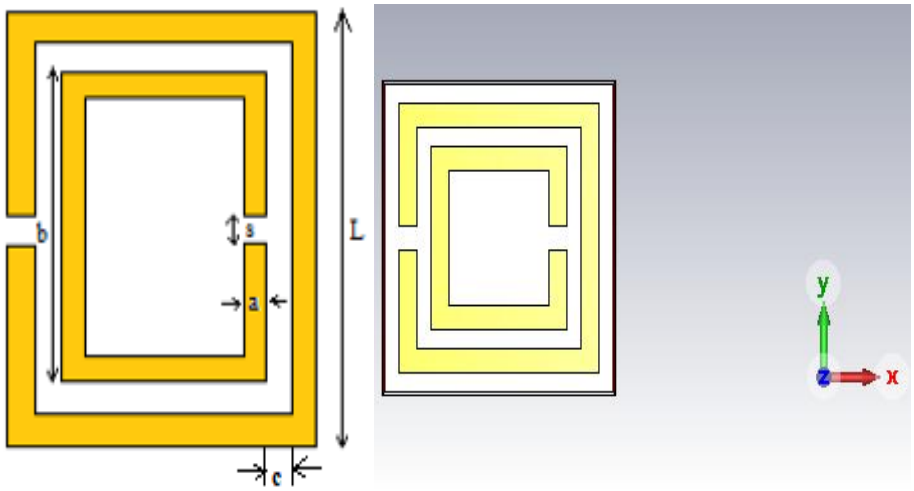

Fig. 5: Unit-cell metamaterial - SSSR (a) Schematic diagram (b) Unit cell in CST MWS

International Journal of Advances in Engineering and Management (IJAEM)
Volume 6, Issue 10 Oct. 2024, pp: 214-229www.ijaem.net ISSN: 2395-5252

Table 2: Dimensions of proposed antenna with unit cell MTM

Parameter	Value (mm)
Lg	5.45
Wg	6.28
Lp	3.41
Wp	4.24
t	0.035
h	0.34
yo	1.19
g	0.14
L_f	0.51
W_f	3.04
L	1.00
s	0.10
a	0.10
b	0.60
c	0.10

3.5Proposed antenna with Metamaterial and DGS

To achieve the desired surface current distribution, impedance bandwidth and resonation properties, the structure presented in Fig. 4 was modified by introducing a MTM structure (SSRR) on the primary patch and defected ground structure (DGS) on the ground plane. The position and size of the DGS on the ground plane was taken to be the mirror image of the primary patch on the ground plane and finetuned on CST studio. The modified structure is presented in Fig.6. The optimised dimension (length, width and height) of the patch are$2.8 \times 3 \times 0.34\ mm^3$.

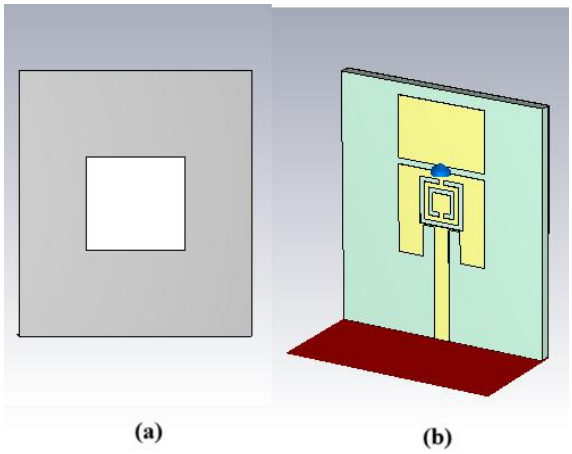

Fig. 7: Proposed MTM-based antenna in CST MWS (a) Top view (b) Bottom view

IV. RESULTS AND DISCUSSION

Essential antenna parameters such as impedance bandwidth, radiation pattern, VSWR, directivity, gain and return loss, will be extracted from the simulated results to analyse the proposed antenna.

4.1Return Loss Plots and Impedance Bandwidth of Designed Antennas

Figs.8 to 12depict the return loss plots of the single-band antennas that were designed in section 3.0, as well as the return loss graph of the proposed antenna in both its diode ON and OFF states. The antennas resonated at frequencies of 26, 28, and 30 GHz corresponded to minimal return loss values of -40.18, -25.11, and -18.05 dB,

International Journal of Advances in Engineering and Management (IJAEM)
Volume 6, Issue 10 Oct. 2024, pp: 214-229www.ijaem.net ISSN: 2395-5252

respectively, as shown in Figs.8 to 10. The single-band antennas showed bandwidths of 694, 902, and 908 MHz at frequencies of 26, 28, and 30 GHz, respectively.

Figs.11 and 12 depict the return loss plots of the proposed antenna's two-state operation modes. The results demonstrated bandwidth coverage across the designed frequencies. When the diode was turned on, a minimum return loss of -25.37 dB wasobtained at a resonance frequency of 28.78 GHz. Additionally, a bandwidth of 2.56 GHz was recorded. On the other hand, as shown in Fig.12, when the diode was deactivated, a minimum return loss of -24.3 dB was obtained at a resonance frequency of 27.09 GHz. The antenna achieved an impedance bandwidth performance of 2.23 GHz.

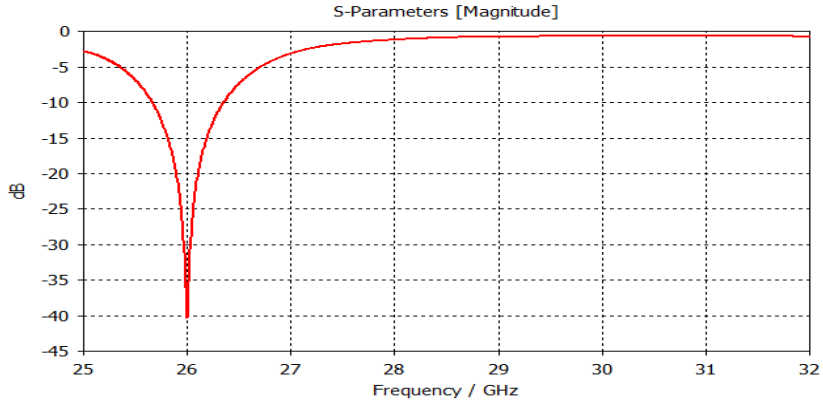

Fig.8: 26 GHz single-band antenna return loss plot

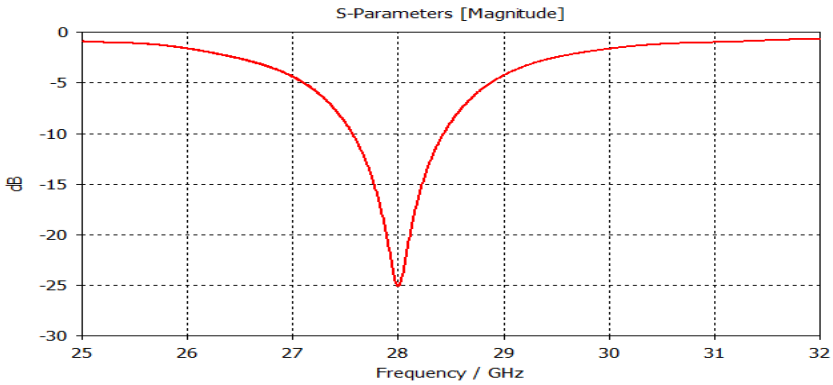

Fig.9: 28 GHz single-band antenna return loss plot

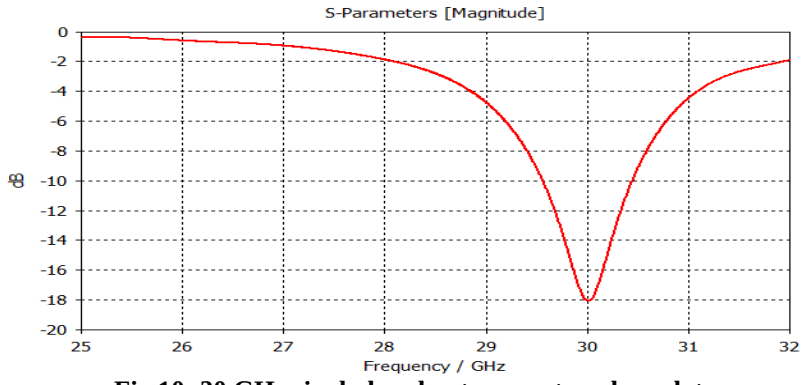

Fig.10: 30 GHz single-band antenna return loss plot

International Journal of Advances in Engineering and Management (IJAEM)
Volume 6, Issue 10 Oct. 2024, pp: 214-229www.ijaem.net ISSN: 2395-5252

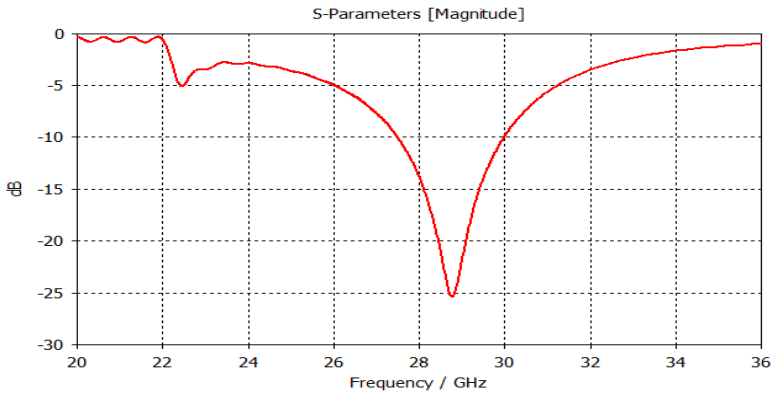

Fig.11: Proposed antenna return loss (diode ON)

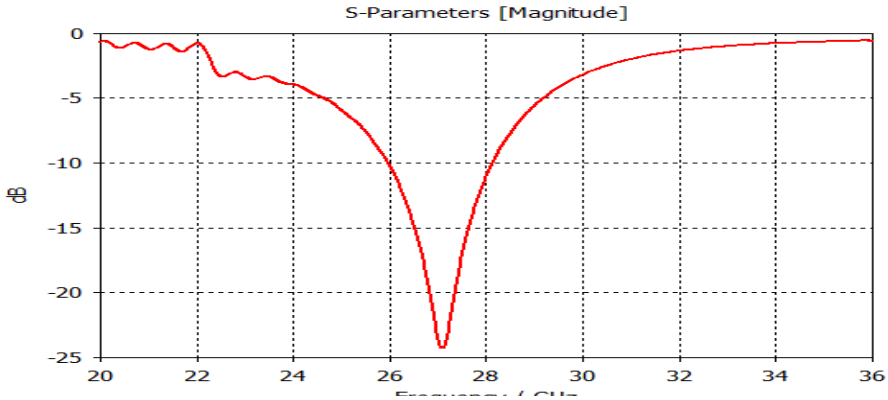

Fig.12: Proposed antenna return loss (diode OFF)

4.2Voltage Standing Wave Ratio (VSWR) and Gain of the Designed Antenna

Voltage standing wave ratio (VSWR) is an indicator used to determine if an antenna has the correct impedance matching. In order to obtain a proper impedance match, the VSWR of an antenna should be between 1 and 2, meaning that $1 \leq VSWR \leq 2$[21]. Additionally, the closer the VSWR is to 1, the more accurate the impedance match will be at the resonance frequency. Figs.13to 15 depict the VSWR of single-band antennas at frequencies of 26, 28, and 30 GHz. It is evident that all the single-band antennas met the requirement for a favourable impedance match, with values of 1.02, 1.12, and 1.29 at resonance.

The VSWR plots of the suggested antenna may be seen in Figs.16 and 17. These figures show that the corresponding lowest return loss values are observed at VSWR values of 1.13 and 1.11, respectively.

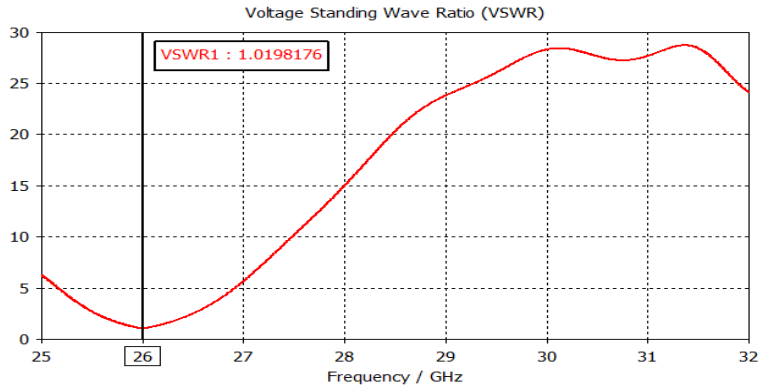

Fig.13: VSWR of MSA at 26 GHz

International Journal of Advances in Engineering and Management (IJAEM)
Volume 6, Issue 10 Oct. 2024, pp: 214-229www.ijaem.net ISSN: 2395-5252

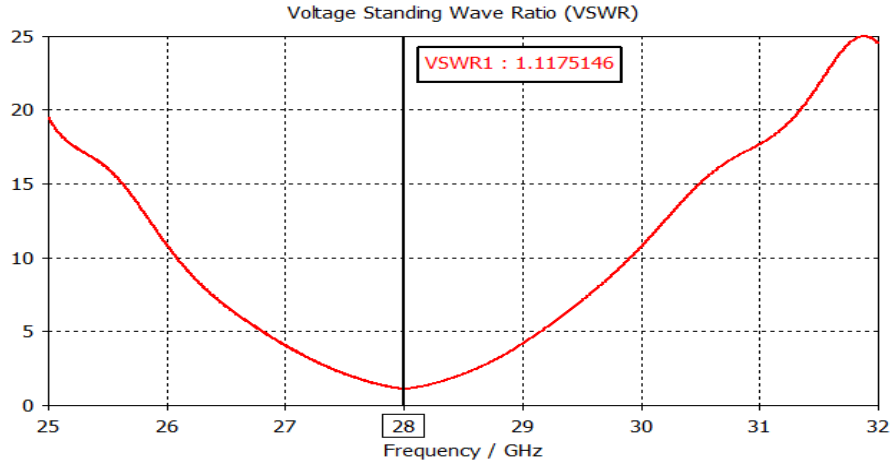

Fig.14: VSWR of MSA at 28 GHz

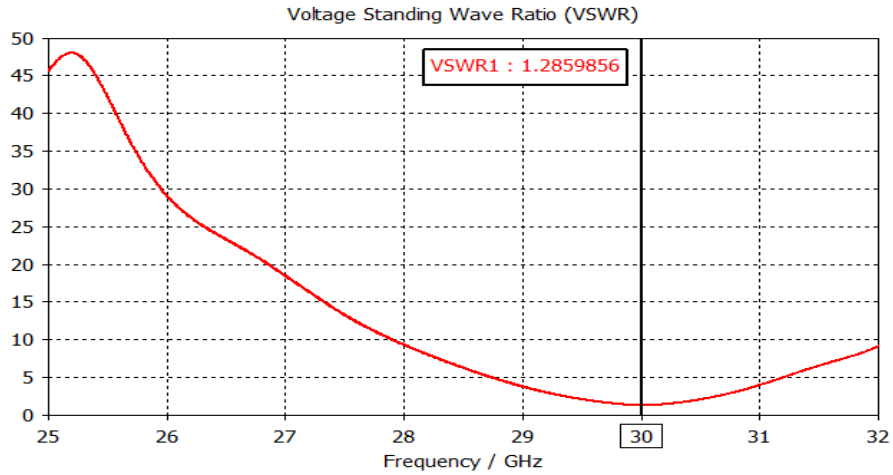

Fig.15: VSWR of MSA at 30 GHz

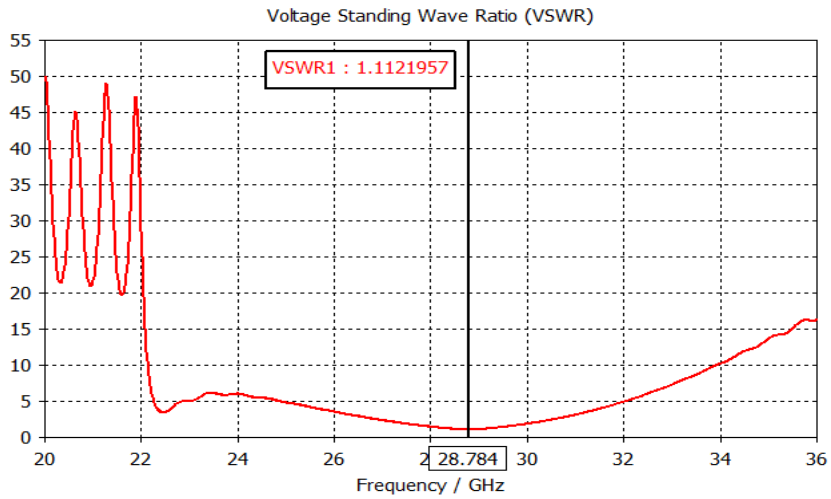

Fig.16: VSWR of proposed reconfigurable MTM antenna (diode ON)

International Journal of Advances in Engineering and Management (IJAEM)
Volume 6, Issue 10 Oct. 2024, pp: 214-229www.ijaem.net ISSN: 2395-5252

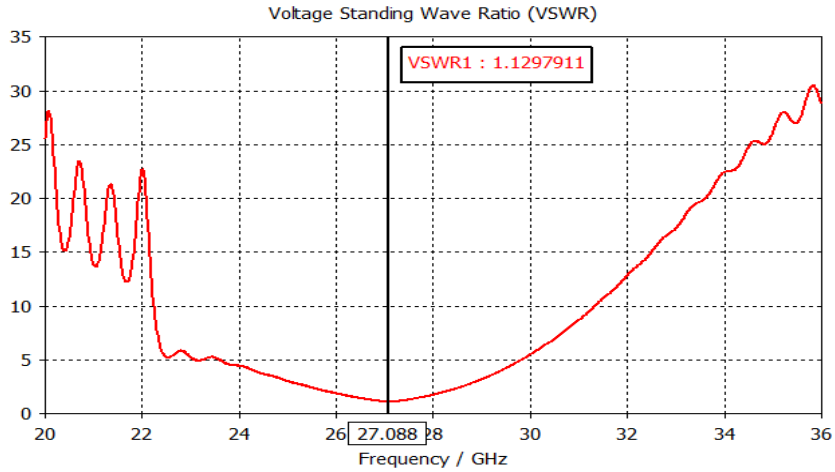

Fig.17: VSWR of proposed reconfigurable MTM antenna (diode OFF)

4.3Field Regions, Directivity and Radiation Pattern

According [22] and [23], the electromagnetic field generated by an antenna is divided into two or three distinct regions, known as the far-field, reactive near-field, and Fresnel zones. These regions are seen in Fig.18. Nevertheless, considering the dimensions of the microstrip antennas under investigation in this paper, it was found that the reactive near-field region was the most prominent area.

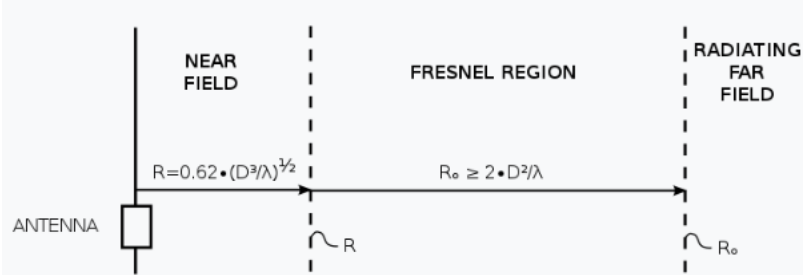

Fig.18: Antenna regions according to diffraction behaviour[23]

Far-field: The measured point at which the radiating field components are substantial is within a short distance $(3\ m)$ to regions surrounding the device under test (DUT).

Reactive near field: Microstrip array antennas are often classified as electrically large antennas according to the Chu limit, unless specifically constructed to be otherwise. The reactive near field distance, denoted as R, for the antenna under consideration is determined mathematically using Equation 18, which has been derived from the work of Ziolkowski and Erentok (2007). The calculation is performed as follows:

$$R < 0.62\sqrt{\frac{D^3}{\lambda}} \qquad (18)$$

where D is the largest size of the patch and $\lambda = \lambda_{air}$ is the wavelength.

Substituting D = 40 mm, $\lambda_{air\ (at\ 28\ GHz)} = 10.71\ mm$;

$$R \leq 0.62\sqrt{\frac{40^3}{10.71}} = 47.93\ mm$$

This indicates that for the proposed antenna, the reactive near-field region is observed to be $\leq 47.93\ mm$ ($\approx 4.48\lambda_{air}$).

Fresnel region: No definite Fresnel region measurement was observed during the simulation of the proposed antenna. However, given the dimensions of the antenna in comparison to the highest value of wavelength obtained, the outer boundary of the radiating near field may be approximated from Equation 19 as follows:

$$R \approx \frac{2D^2}{\lambda} \qquad (19)$$

$$\approx \frac{2 \times 40^2}{10.71} \approx 300\ mm$$

This shows that the far-field region (3 m) previously projected for the proposed antenna was not in order since the Fresnel region spans below 3 m. Note that the Fresnel region is the region between an antenna's far field and the reactive near

International Journal of Advances in Engineering and Management (IJAEM)
Volume 6, Issue 10 Oct. 2024, pp: 214-229www.ijaem.net ISSN: 2395-5252

field. The value of *R* computed for the Fresnel region is the primary reason for the adoption of multiple repeaters for the deployment of 5G signal at millimetre wave frequencies.

The polar plots of the H-plane and E-plane antenna and directivity patterns of the proposed reconfigurable microstrip antenna are given in Figs.19 to 21. From the directivity plots, a slight shift in characteristics, as expected, is observable, especially at the higher frequencies of 28 and 30 GHz. HPBW and side lobe levels were not left out in the behavioural change noted concerning uniformity in reflected wave noticeable at 28 and 30 GHz.

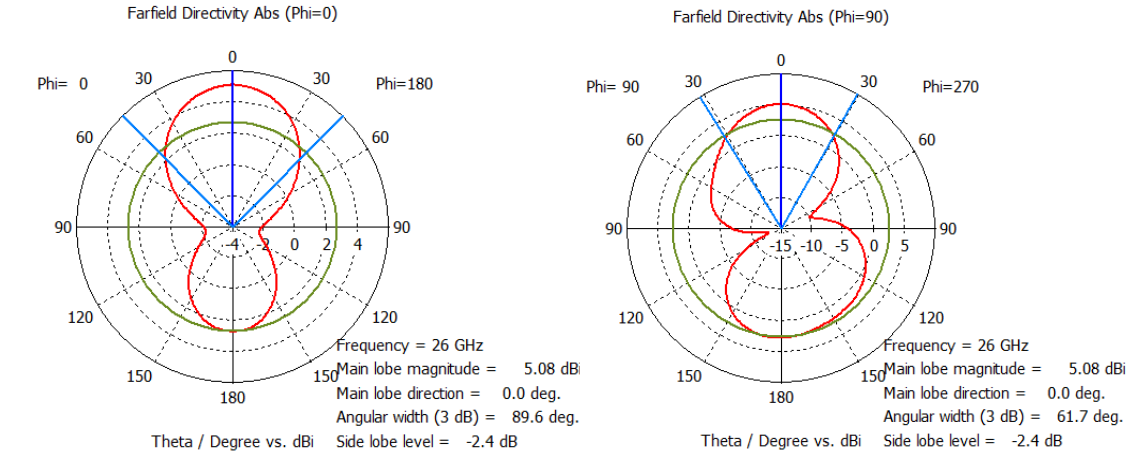

(a) **(b)**

Fig. 19: Directivity plot of proposed antenna at 26 GHz with diode OFF (a) E-plane (b) H-plane

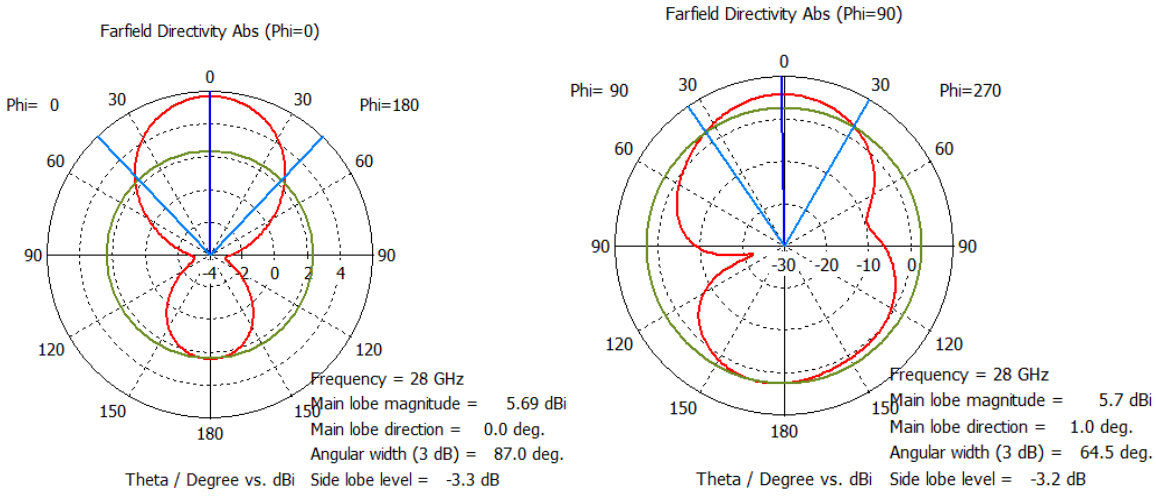

(a) **(b)**

Fig. 20: Directivity plot of proposed antenna at 28 GHz with diode OFF (a) E-plane (b) H-plane

International Journal of Advances in Engineering and Management (IJAEM)
Volume 6, Issue 10 Oct. 2024, pp: 214-229www.ijaem.net ISSN: 2395-5252

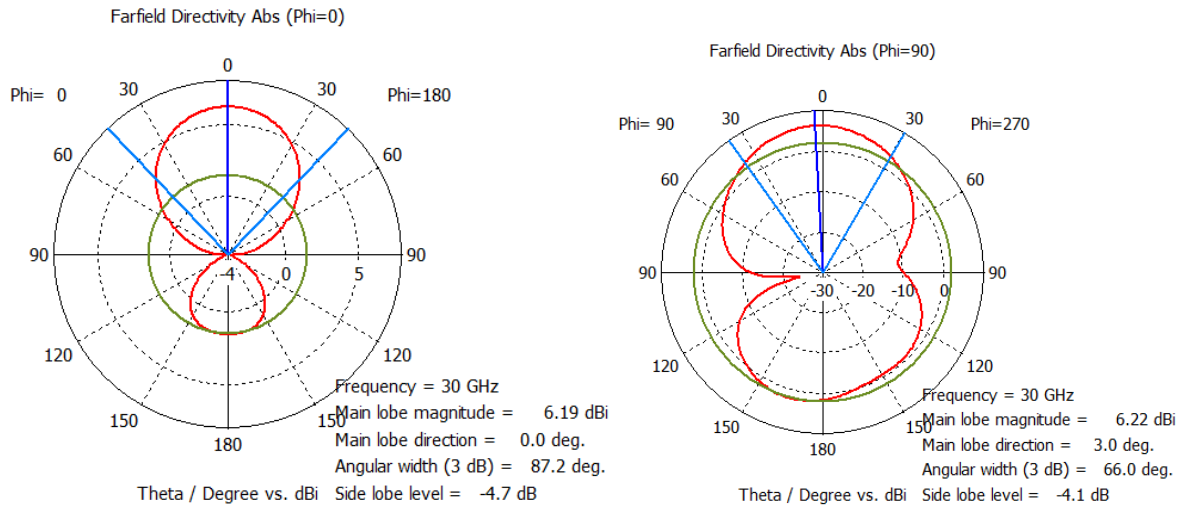

Fig.21: Directivity plot of proposed antennaat 30 GHz with diode OFF (a) E-plane (b) H-plane

In terms of radiation pattern, all single-band antennas designed in this study exhibited directional radiation patterns in the E-plane and a nearly omnidirectional pattern in the H-plane. Similar attributes were observed on the proposed antenna, with further deviations at 28 and 30 GHz.

4.4Gain of the Designed Antenna

Predominantly, miniaturized antennas (mainly found in compact mobile devices), as stated by[24], are affected by poor antenna efficiency, with planar inverted-F antennas (PIFA) being a good example. Antenna gains of 3.75, 4.47, and 5.06 dBi were achieved at 26, 28, and 30 GHz by the proposed reconfigurable antenna with diode ON, as illustrated in Figs.22 to 24. These values represent a 24% average decrease from single-band antennas at similar resonance frequencies.

Similar characteristics were observed when the diode is switched OFF in that a decrease was equally noticeable though minimal (11%), as illustrated in Figs.25 to 27. Antenna gain values of 4.48, 5.19, and 5.74 were achieved at corresponding resonance frequencies of 26, 28, and 30 GHz.

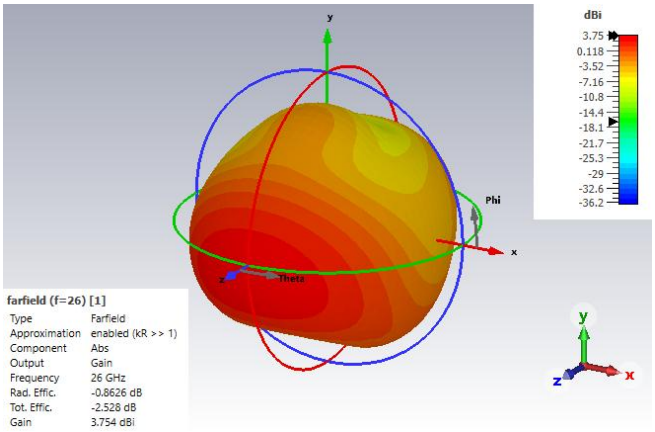

Fig.22: Gain of proposed reconfigurable antenna at 26 GHz (diode ON)

International Journal of Advances in Engineering and Management (IJAEM)
Volume 6, Issue 10 Oct. 2024, pp: 214-229www.ijaem.net ISSN: 2395-5252

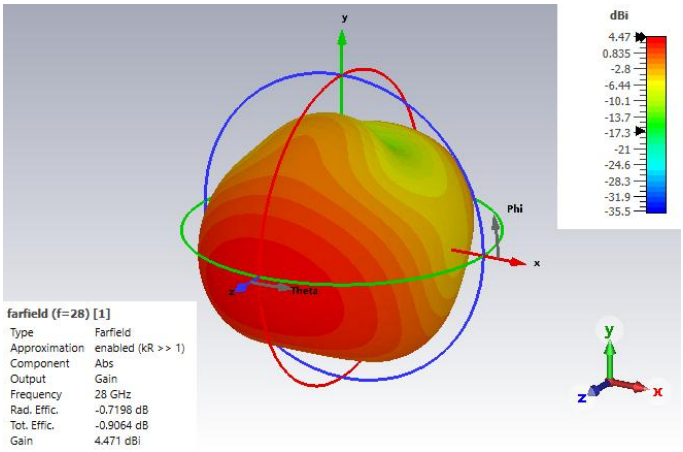

Fig.23: Gain of proposed reconfigurable antenna at 28 GHz (diode ON)

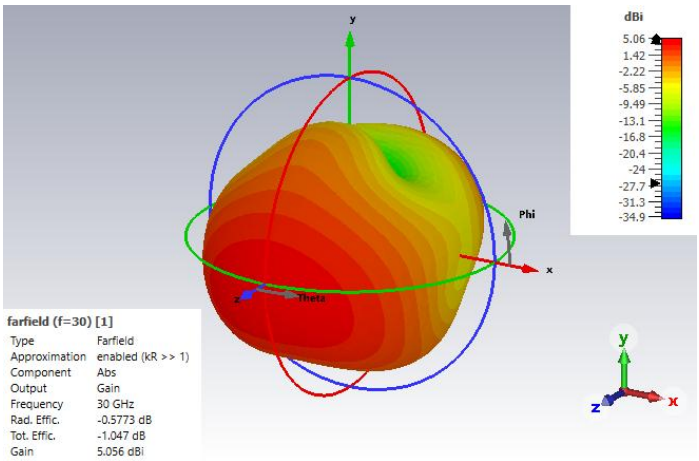

Fig.24: Gain of proposed reconfigurable antenna at 30 GHz (diode ON)

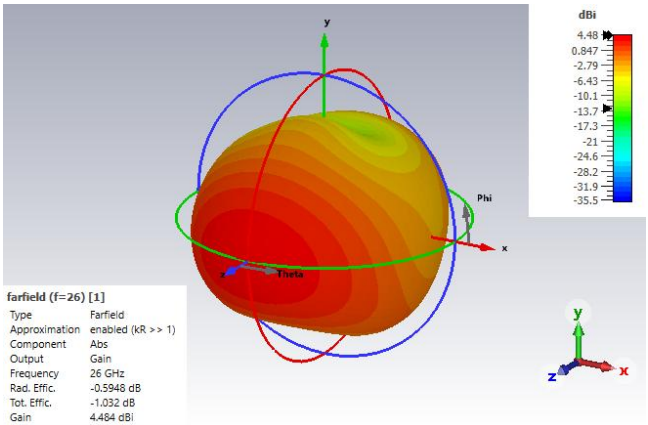

Fig.25: Gain of proposed reconfigurable antenna at 26 GHz (diode OFF)

International Journal of Advances in Engineering and Management (IJAEM)
Volume 6, Issue 10 Oct. 2024, pp: 214-229www.ijaem.net ISSN: 2395-5252

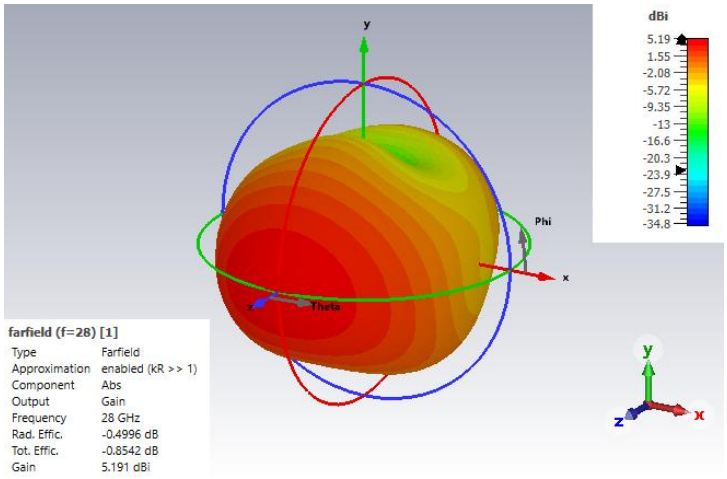

Fig.26: Gain of proposed reconfigurable antenna at 28 GHz (diode OFF)

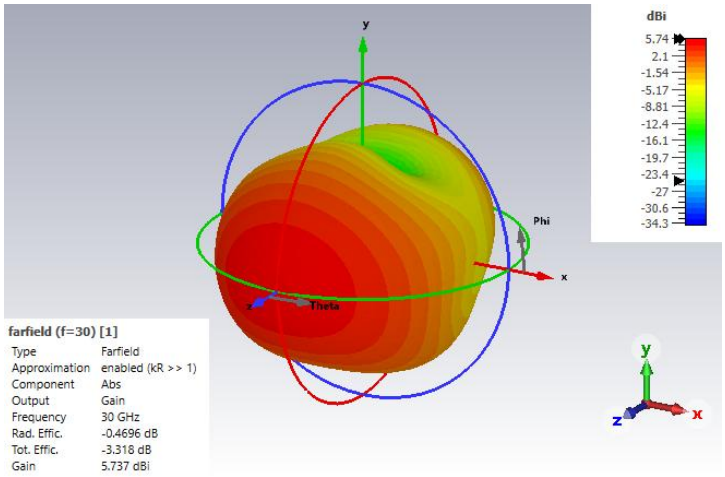

Fig.27: Gain of proposed reconfigurable antenna at 30 GHz (diode OFF)

4.5 Discussion

Critical analysis of the computed and simulated results presented in the previous sections of this paper revealed that bandwidths of 694 MHz, 902 MHz, and 908 MHz at 26 GHz, 28 GHz, and 30 GHz, VSWRs of 1.02, 1.12, and 1.29 were achieved by the single band microstrip antennas. The proposed reconfigurable antenna achieved 2.56 and 2.23 GHz bandwidths when the diode is ON and OFF. These results indicate that the proposed antenna met the objectives outlined for the study.

The reconfigurable rectangular microstrip antenna presented in this work was compared to previously evaluated published journals mentioned in Chapter Two, as well as other similar reconfigurable antennas. In their study,[10] found that their antenna had an impedance bandwidth of 3.5 GHz, whereas the proposed reconfigurable antenna reached a total bandwidth of 4.79 GHz. Table 3 presents a concise overview of performance comparisons. Table 3 clearly shows that while all the assessed works performed satisfactorily, none of them achieved the same level of performance as the proposed MTM-based antenna in terms of bandwidth. The dimensions of the various antennas could only serve as a benchmark for evaluation if they were all functioning at the same frequency. It is crucial to acknowledge that the bandwidth being evaluated is the total impedance bandwidth throughout the frequencies that have been designed.

Table 3: Comparative analysis of the proposed antenna with a few chosen studies from the literature

Antenna	f_r (GHz)	Bandwidth (MHz)
[25]	1.8/3.1/5.8	700
[26]	3.8/5.3/8	1,050
[27]	2.4/3/5.7	42.07%
[28]	2.4/3.5/5.6	264
[10]	30 GHz	3,500
[8]	28 GHz	2,570
[12]	27.8	Nil
[13]	24	Nil
Proposed reconf. RMSA	26/28/30	4,790

V. CONCLUSION

This study focused on the design and performance evaluation of a reconfigurable millimetre-wave (mm-Wave) antenna for 5G technology, targeting frequencies of 26, 28, and 30 GHz. The design includes three single-band microstrip antennas, analysed for return loss, VSWR, radiation pattern, directivity, and gain. A reconfigurable mechanism using diodes enables the antenna to switch between different operational states, adjusting its bandwidth and performance. In the ON state, the antenna achieved a 2.56 GHz bandwidth, while in the OFF state, it achieved 2.23 GHz. This adaptability allows it to meet the varying demands of 5G networks, making it suitable for high-frequency, high-speed applications. The antenna's performance metrics confirm its effectiveness for 5G and beyond technologies.

REFERENCES

[1]. N. O. Parchin et al., Frequency reconfigurable antenna array for MM-wave 5g mobile handsets, vol. 263. Springer International Publishing, 2019. doi: 10.1007/978-3-030-05195-2_43.

[2]. W. A. Awan, “Very small form factor with Ultra Wide Band Rectangular Patch Antenna for 5G Applications,” Int. Conf. Comput. Math. Eng. Technol., pp. 38–41, 2018.

[3]. S. Il Kim, D. H. Kim, T. Van Son, J. Y. Park, D. S. Kim, and K. C. Hwang, “Optimization of Cavity-backed patch array antenna using Genetic Algorithm,” ISAP 2018 - 2018 Int. Symp. Antennas Propag., no. Isap, pp. 529–530, 2018.

[4]. S. Kumar and A. Kumar, “5G New Radio Deployment Modes,” Int. Res. J. Eng. Technol., no. May, pp. 3419–3422, 2020.

[5]. D. Liu, W. Hong, T. S. Rappaport, C. Luxey, and W. Hong, “What will 5G antennas and propagation be?,” IEEE Trans. Antennas Propag., vol. 65, no. 12, pp. 6205–6212, Nov. 2017.

[6]. F. J. Syeda, R. Ardavan, A. Yasir, and A. Akram, “Low-profile flexible frequency-reconfigurable millimetre-wave antenna for 5G applications,” Flex. Print. Electron., vol. 3, no. 3, pp. 1–8, 2018.

[7]. S. H. Kiani et al., “Mimo antenna system for modern 5g handheld devices with healthcare and high rate delivery,” Sensors, vol. 21, no. 21, pp. 1–19, 2021, doi: 10.3390/s21217415.

[8]. D. El Hadri, A. Zakriti, and A. Zugari, “Reconfigurable antenna for Wi-Fi and 5G applications,” Procedia Manuf., vol. 46, no. 2019, pp. 793–799, 2020, doi: 10.1016/j.promfg.2020.04.007.

[9]. A. H. M. Almawgani, “Design and Analysis of Frequency Reconfigurable Antenna for Wideband Millimeter-Wave Communications,” pp. 1–22, 2023.

[10]. S. Kishore and A. R. Abdul Rajak, “Microstrip Patch Antenna with C Slot for 5G Communication at 30 GHz,” Emerg. Sci. J., vol. 6, no. 6, pp. 1315–1327, 2022, doi: 10.28991/ESJ-2022-06-06-06.

[11]. A. H. M. Almawgani, U. Y. Devi, B. T. P. Madhav, and A. R. H. Alhawari, “Design and Analysis of Frequency Reconfigurable Antenna for Wideband Millimeter-Wave Communications,” ResearchSquare, pp. 1–22, 2023.

[12]. B. Alekhya, N. A. Murugan, B. T. P. Madhav, and N. K. R. Reddy, “Millimeter-Wave Reconfigurable Antenna for 5G Wireless Communications,” Prog. Electromagn. Res. Lett., vol. 101, no. July, pp. 107–115, 2021, doi: 10.2528/PIERL21070902.

[13]. O. Lafond et al., “Millimeter wave reconfigurable antenna based on active printed array and inhomogeneous lens,” Proc. 38th Eur. Microw. Conf. EuMC

2008, no. December, pp. 147–150, 2008, doi: 10.1109/EUMC.2008.4751409.

[14]. A. D. Utahile, U. K. Michael, and O. A. Bernard, "Multiband Band and Dual Diversity Eight-Element MIMO Microstrip Antenna for Wireless Applications," J. Eng. Res. Reports, vol. 25, no. 7, pp. 32–42, 2023, doi: 10.9734/jerr/2023/v25i7935.

[15]. C. A. Balanis, Antenna Theory: Analysis and Design., 4th ed. New Jersey: John Wiley & Sons, 2016.

[16]. J. R. Reis, M. Vala, T. E. Oliveira, T. R. Fernandes, and R. F. S. Caldeirinha, "Metamaterial-inspired flat beamsteering antenna for 5g base stations at 3.6 ghz," Sensors, vol. 21, no. 23, pp. 1–14, 2021, doi: 10.3390/s21238116.

[17]. P. Z. H. Cano, Z. D. Zaharis, T. V. Yioultsis, N. V. Kantartzis, and P. I. Lazaridis, "Pattern Reconfigurable Antennas at Millimeter-Wave Frequencies: A Comprehensive Survey," IEEE Access, vol. 10. Institute of Electrical and Electronics Engineers Inc., pp. 83029–83042, 2022. doi: 10.1109/ACCESS.2022.3196456.

[18]. K. Veerendra, G. P. Ratna, and S. N. Bhavanam, "Design of Microstrip Patch Antenna with Parasitic Elements for Wideband Applications," Int. J. Innov. Res. Technol., vol. 6, no. 2, pp. 324–327, 2019, [Online]. Available: https://www.researchsquare.com/article/rs-1477458/latest.pdf

[19]. S. S. Rani and K. K. Naik, "Design and Analysis of Complimentary Split Ring Resonator with Slot on Retangular Patch Antenna for Wireless Applications," Int. J. Recent Technol. Eng., vol. 7, no. 6, pp. 50–53, 2019.

[20]. N. Abdullah, G. Bhardwaj, and Sunita, "Design of squared shape SRR metamaterial by using rectangular microstrip patch antenna at 2.85 GHz," 2017 4th Int. Conf. Signal Process. Integr. Networks, SPIN 2017, pp. 196–200, 2017, doi: 10.1109/SPIN.2017.8049943.

[21]. A. Bellekhiri, N. Chahboun, Y. Laaziz, and A. El Oualkadi, "A new design of 5G planar antenna with enhancement of the bandwidth and the gain using metasurface," E3S Web Conf., vol. 351, pp. 1–5, 2022, doi: 10.1051/e3sconf/202235101054.

[22]. M. Sohail and R. Uyguroğlu, "Near Field Focused Microstrip Patch Antenna Array Characteristics Enhancement With Parasitic Patch Elements," in 2021 29th Signal Processing and Communications Applications Conference (SIU), Istanbul, Turkey, 2021, pp. 1–4.

[23]. A. Z. Elsherbeni and V. Demir, The finite-difference time-domain for Electromagnetics : with MATLAB simulations, 2nd ed. Institution of Engineering and Technology, 2016. Accessed: Feb. 03, 2023. [Online]. Available: https://books.google.com/books/about/The_Finite_difference_Time_domain_for_El.html?id=09FYnQAACAAJ

[24]. S. Kumar, A. S. Dixit, R. R. Malekar, H. D. Raut, and L. K. Shevada, "Fifth generation antennas: A comprehensive review of design and performance enhancement techniques," IEEE Access, vol. 8, pp. 163568–163593, 2020, doi: 10.1109/ACCESS.2020.3020952.

[25]. C. Zhu, Z. Su, X. Dang, H. Zhai, L. Li, and C. Liang, "A CPW-Fed Triple Band Metamaterial Antenna with TER and CTER Loading," IEEE Antennas Propag. Lett., vol. 1, pp. 3–6, 2014.

[26]. T. Saeidi et al., "High Gain Triple-Band Metamaterial-Based Antipodal Vivaldi MIMO Antenna for 5G Communications," Micromachines 2021, Vol. 12, Page 250, vol. 12, no. 3, p. 250, Feb. 2021, doi: 10.3390/MI12030250.

[27]. S. K. Sharma, J. D. Mulchandani, D. Gupta, and R. K. Chaudhary, "Triple-band metamaterial-inspired antenna using FDTD technique for WLAN/WiMAX applications," Int. J. RF Microw. Comput. Eng., vol. 25, no. 8, pp. 688–695, Oct. 2015, doi: 10.1002/MMCE.20907.

[28]. E. K. I. Hamad, W. A. E. Ali, M. Z. M. Hamdalla, and M. A. Bassiuny, "High gain triple band microstrip antenna based on metamaterial super lens for wireless communication applications," Proc. 2018 Int. Conf. Innov. Trends Comput. Eng. ITCE 2018, vol. 2018-March, pp. 197–204, Mar. 2018, doi: 10.1109/ITCE.2018.8316624.